Published in final edited form as:
Dev Cell. 2013 November 25; 27(4): 425–437. doi:10.1016/j.devcel.2013.10.007.

Self-Assembly of VPS41 Promotes Sorting Required for Biogenesis of the Regulated Secretory Pathway

Cédric S. Asensio[1,2], **Daniel W. Sirkis**[1,2], **James W. Maas Jr.**[1,2], **Kiyoshi Egami**[3], **Tsz-Leung To**[4], **Frances M. Brodsky**[5,6,7], **Xiaokun Shu**[4], **Yifan Cheng**[3], and **Robert H. Edwards**[1,2,*]

[1]Department of Physiology, University of California, San Francisco, San Francisco, CA 94158, USA

[2]Department of Neurology, University of California, San Francisco, San Francisco, CA 94158, USA

[3]W.M. Keck Advanced Microscopy Laboratory, Department of Biochemistry and Biophysics, University of California, San Francisco, San Francisco, CA 94158, USA

[4]Cardiovascular Research Institute, Department of Pharmaceutical Chemistry, University of California, San Francisco, San Francisco, CA 94158, USA

[5]G.W. Hooper Foundation, Department of Bioengineering and Therapeutic Sciences, University of California, San Francisco, San Francisco, CA 94158, USA

[6]Department of Pharmaceutical Chemistry, University of California, San Francisco, San Francisco, CA 94158, USA

[7]Department of Microbiology and Immunology, University of California, San Francisco, San Francisco, CA 94158, USA

SUMMARY

The regulated release of polypeptides has a central role in physiology, behavior, and development, but the mechanisms responsible for production of the large dense core vesicles (LDCVs) capable of regulated release have remained poorly understood. Recent work has implicated cytosolic adaptor protein AP-3 in the recruitment of LDCV membrane proteins that confer regulated release. However, AP-3 in mammals has been considered to function in the endolysosomal pathway and in the biosynthetic pathway only in yeast. We now find that the mammalian homolog of yeast VPS41, a member of the homotypic fusion and vacuole protein sorting (HOPS) complex that delivers biosynthetic cargo to the endocytic pathway in yeast, promotes LDCV formation through a common mechanism with AP-3, indicating a conserved role for these proteins in the biosynthetic pathway. VPS41 also self-assembles into a lattice, suggesting that it acts as a coat protein for AP-3 in formation of the regulated secretory pathway.

INTRODUCTION

The function of peptide hormones, neural peptides, and many growth factors depends on their regulated release in response to a physiologically appropriate stimulus. However, the mechanisms responsible for sorting polypeptides into a secretory pathway capable of

*Correspondence: robert.edwards@ucsf.eduhttp://dx.doi.org/10.1016/j.devcel.2013.10.007.

SUPPLEMENTAL INFORMATION

Supplemental Information includes Supplemental Experimental Procedures, four figures, and one table and can be found with this article online at http://dx.doi.org/10.1016/j.devcel.2013.10.007.

regulated release, and indeed for biogenesis of this pathway, remain poorly understood. In contrast to the proteins released constitutively after biosynthesis, proteins destined for regulated secretion undergo storage within secretory granules or large dense core vesicles (LDCVs) competent for regulated exocytosis. LDCVs form at the *trans*-Golgi network (TGN), where their soluble cargo aggregate to form a dense core (Orci et al., 1987; Tooze and Huttner, 1990; Eaton et al., 2000), suggesting that lumenal interactions drive sorting to LDCVs and their formation (Kim et al., 2001; Turkewitz, 2004). Several components of the dense core indeed reproduce the morphology of LDCVs when expressed in nonneuroendocrine cells (Kim et al., 2001, 2005), but the LDCVs formed under these circumstances lack the capacity for regulated release, presumably because they do not contain the required membrane proteins. In addition, LDCVs undergo a process of maturation during which proteins eventually localizing to other organelles are removed (Arvan and Castle, 1998; Morvan and Tooze, 2008). Thus, LDCVs might form simply through the removal of components that promote constitutive release, leaving those that enable regulated secretion. However, maturation is not required for regulated release in at least some neuroendocrine cells (Tooze et al., 1991). In addition, metabolic labeling experiments have demonstrated that constitutive and regulated cargo segregate into distinct vesicles upon budding from the TGN (Tooze and Huttner, 1990). Thus, LDCVs appear to form through a specific sorting event that, similar to other trafficking events in the cell, may involve cytosolic machinery.

Consistent with a role for cytosolic machinery in biogenesis of the regulated secretory pathway, several membrane proteins contain cytoplasmic sequences required for their sorting to LDCVs (Blagoveshchenskaya et al., 1999, 2002; El Meskini et al., 2001). Both vesicular monoamine transporter 2 (VMAT2) and the inactive transmembrane phosphatase IA-2β (phogrin) sort to LDCVs dependent on a cytoplasmic dileucine-like motif with upstream acidic residues flanked by basic residues (Krantz et al., 2000; Torii et al., 2005), similar to the signals recognized by known clathrin adaptor proteins (Robinson and Bonifacino, 2001). However, clathrin is not required for regulated release (Molinete et al., 2001), and LDCVs budding from the TGN do not exhibit a recognizable coat. The cytosolic machinery responsible for LDCV formation at the Golgi apparatus has thus remained unknown.

Mutation of the dileucine-like motif in VMAT2 increases cell surface expression due to diversion of the transporter from regulated to constitutive secretory pathway (Tan et al., 1998; Li et al., 2005). We have therefore used RNAi to screen for genes that increase surface expression of the wild-type transporter and so phenocopy the effect of this mutation. Performed in *Drosophila* S2 cells, the screen identified multiple subunits of the cytosolic adaptor protein AP-3 (Asensio et al., 2010). In mammalian neuroendocrine PC12 cells, loss of AP-3 disrupts sorting to the regulated secretory pathway, dysregulates the release of soluble cargo, and indeed impairs the formation of LDCVs (Asensio et al., 2010). Reduced in number and larger than normal (Grabner et al., 2006), LDCVs still form in the absence of AP-3, but show changes in the composition of membrane proteins (such as the calcium sensor synaptotagmin) required for regulated exocytosis (Asensio et al., 2010). AP-3 thus directs formation of the regulated secretory pathway.

Our understanding of AP-3 is derived from two main sources. In mammalian systems, AP-3 has been considered to function only within the endolysosomal pathway, in trafficking from early endosomes to lysosomes, synaptic vesicles and lysosome-related organelles (LROs) such as melanosomes (Faúndez et al., 1998; Raposo and Marks, 2007; Dell'Angelica, 2009). The identification of a role for AP-3 in LDCV formation at the Golgi complex (Asensio et al., 2010), and hence in the bio-synthetic pathway, was therefore quite surprising. On the other hand, genetic analysis in *Saccharomyces cerevisiae* has indicated a role for AP-3 in the

delivery of membrane proteins from the biosynthetic pathway to the yeast lysosome, or vacuole (Cowles et al., 1997; Odorizzi et al., 1998), but this has been attributed to a fundamental difference between yeast and mammals. The identification of a role for AP-3 in LDCV formation by mammalian cells has thus revealed a function that may be related to its role in yeast. Interestingly, studies in yeast have shown that several proteins associated with AP-3 also contribute to the biosynthetic pathway, but their function in mammals has remained unknown.

RESULTS

VPS41 Is Required for Sorting to the Regulated Secretory Pathway in *Drosophila* S2 Cells

To understand how AP-3 contributes to formation of the regulated secretory pathway, we examined other proteins with which it has been suggested to associate (Table S1 available online), even though most of these have been implicated in the endolysosomal rather than biosynthetic pathway of mammalian cells. Taking advantage of the flow cytometry-based assay developed to assess the surface expression of *Drosophila* VMAT (dVMAT) in S2 cells (Asensio et al., 2010), we found that only RNAi directed against the vacuolar protein sorting gene *vps41*, a subunit of the homotypic fusion and vacuolar protein sorting (HOPS) complex (Angers and Merz, 2009; Cabrera et al., 2009; Plemel et al., 2011), increases the surface expression of dVMAT (Figure S1A). The increase in surface dVMAT produced by VPS41 dsRNA suggests diversion from the regulated to constitutive pathway, but is nonetheless small relative to the effects of AP-3 dsRNA (Figure S1A) (Asensio et al., 2010), presumably accounting for the failure to identify *vps41* in the original screen (Asensio et al., 2010). To determine whether VPS41 contributes to the regulated release of soluble cargo, we transfected the S2 cells with the peptide hormone atrial natriuretic factor fused to GFP (ANF-GFP) that we have shown to undergo regulated, Ca^{2+}-dependent release from these *Drosophila* cells in response to stimulation with lipopolysaccharide (LPS) (Asensio et al., 2010). We find that dsRNA to VPS41 both profoundly impairs the stimulated secretion of ANF-GFP and increases its constitutive release (Figures S1B and S1C). Similar to AP-3, VPS41 thus appears required for sorting to the regulated secretory pathway in *Drosophila* S2 cells.

The small effect of VPS41 RNAi on surface expression of dVMAT suggested that other HOPS complex subunits might have a similarly disproportionate role in the regulated release of soluble cargo. However, dsRNA to VPS18, a core component of the HOPS complex required for its assembly (Nickerson et al., 2009), has no effect on the release of ANF-GFP stimulated by LPS (Figure S1B), suggesting an independent and thus highly specific role for VPS41. Because the HOPS and biogenesis of lysosome-related organelle (BLOC) complexes have, like AP-3, been implicated in trafficking from endosomes to lysosomes or LROs in metazoans (Dell'Angelica, 2009; Newell-Litwa et al., 2009), the failure of RNAi directed against them to increase surface expression of dVMAT or dysregulate secretion of ANF-GFP further suggests that the role of AP-3 and VPS41 in sorting to the regulated pathway does not involve their established function in endocytic pathways.

VPS41 Is Required for the Biogenesis of LDCVs in Mammalian Cells

To assess a role for VPS41 in sorting to the regulated pathway of mammals, we knocked down its expression in neuroendocrine PC12 cells. Using siRNA that reduces the expression of myc-tagged VPS41 in COS7 cells (Figure S1D), we find an increase in VMAT2 surface expression similar to that obtained with AP-3 RNAi but smaller than that produced by the EE/AA mutation that redirects the transporter from regulated to constitutive secretory pathway (Li et al., 2005) (Figure 1A). VPS41 RNAi also causes a substantial defect in the release of endogenous secretogranin II (SgII) in response to depolarization with 90 mM K^+

(Figures 1B and 1C). Like the knockdown of AP-3, VPS41 RNAi also reduces cellular secretogranin levels (Figures 1B and 1D), which would increase the amount of constitutive release if normalized to the cellular content.

We also used transfection of soluble cargo ANF-GFP to determine whether an RNAi-resistant form of VPS41 can rescue the effects of VPS41 siRNA in PC12 cells. Because transfection of VPS41 is less efficient than the siRNA, ANF-GFP enabled us to assess rescue specifically in the cotransfected cells. The effect of VPS41 RNAi is less profound when using a transfected reporter for soluble cargo such as ANF-GFP, but VPS41 siRNA clearly impairs the regulation of ANF-GFP release (Figure 1E). We find that cotransfecting an RNAi-resistant form of VPS41 completely rescues the defect in regulated release (Figure 1E), excluding off-target effects of the siRNA.

In yeast, VPS41 associates with the HOPS complex, which mediates trafficking from the biosynthetic pathway to the lysosome. The HOPS complex contains four core components shared with the endosomal class C core vacuole/endosome tethering (CORVET) complex along with two HOPS-specific subunits, VPS39 and 41 (Angers and Merz, 2009; Cabrera et al., 2009; Plemel et al., 2011; Swetha et al., 2011). Although the analysis in S2 cells did not reveal a role for other HOPS subunits in sorting to the regulated pathway, we also knocked down in PC12 cells two components of the core complex (VPS11 and 18) and HOPS-specific subunit VPS39. In contrast to RNAi directed against VPS41 (Figure 1F), knock down of VPS11, VPS18, and VPS39 (Figures S1E and S1F) has no effect on the regulation of ANF-GFP release (Figure 1G), supporting a specific role for VPS41, independent of the HOPS complex. To confirm that loss of these proteins has the expected effect on lysosomal function, we measured procathepsin D, a lysosomal prohydrolase that accumulates with lysosome impairment. Figure 1H shows that procathepsin D levels rise in the presence of protease inhibitors and that RNAi to either VPS39 or VPS41 increases procathepsin D to intermediate levels. The loss of either protein thus impairs lysosomal function but only the loss of VPS41 affects regulated secretion, arguing against nonspecific effects of lysosomal dysfunction on the regulated pathway and supporting a role for VPS41 independent of the HOPS complex. In addition, we find that loss of VPS41, but not VPS39, reduces the levels of SgII (Figure 1H), indicating that this aspect of the phenotype also reflects a disturbance in the regulated secretory rather than endolysosomal pathway. Among AP-3-associated proteins and even other HOPS complex subunits, VPS41 thus has a very specific role in formation of the regulated secretory pathway.

VPS41 Influences the Biochemical Properties and Morphology of LDCVs

To determine whether VPS41 is required for the formation of LDCVs, we first used biochemical fractionation. Separating PC12 cell membranes by equilibrium sedimentation through sucrose, we find that SgII still resides in more dense fractions after knock down of VPS41 (Figure 2A). However, the amounts of SgII are greatly reduced, consistent with the decrease in cellular SgII content (Figures 1D and 1H). In addition, the proportion of SgII immunoreactivity in typical LDCV fractions is reduced relative to control cells, and the fractions containing SgII are shifted upward in the gradient (Figure 2A). In separate experiments, cotransfected ANF-GFP shows a similar reduction after VPS41 RNAi, with more of the fusion in lighter fractions (Figure 2D). Remarkably, we observed the same phenotype (reduced soluble cargo and LDCVs shifted upward in the gradient) with AP-3 RNAi (Asensio et al., 2010).

To assess the effect of VPS41 knockdown on a membrane protein of LDCVs, we examined the calcium sensor synaptotagmin 1. Synaptotagmin 1 shows a dramatic redistribution toward much lighter fractions with VPS41 RNAi (Figure 2B), again similar to the effect observed after knockdown of AP-3 (Asensio et al., 2010). Analysis of the membrane protein

synaptophysin shows no effect of VPS41 RNAi (Figure 2C), consistent with the localization of this protein to synaptic-like microvesicles rather than LDCVs (Bauerfeind et al., 1995). VPS41 thus contributes specifically to the formation of LDCVs, influencing their density and composition including membrane proteins as well as soluble cargo.

We then used electron microscopy (EM) to determine whether VPS41 RNAi affects LDCV morphology. The analysis shows a striking reduction in the number and density of LDCVs in PC12 cells subjected to knockdown of VPS41 with both sequences (Figure 3A). In addition, the size of LDCVs appears substantially larger after VPS41 RNAi (Figure 3B). The size of the core shows no change, resulting in LDCVs with a relatively large halo surrounding the core (Figure 3B). Presumably, the increased size of LDCVs after VPS41 RNAi accounts for their reduced density by equilibrium sedimentation (Figure 2A). The reduced number and increased size of LDCVs after VPS41 RNAi again exhibit a striking similarity to the phenotype observed with AP-3 deficiency (Grabner et al., 2006; Asensio et al., 2010), showing that like AP-3, VPS41 contributes to the formation of LDCVs as well as sorting to the regulated pathway. Although the original identification of a role for AP-3 in LDCV formation was surprising given its established function within the endolysosomal pathway of mammals, we thus find that an AP-3-associated protein has the same effect.

VPS41 Interacts with AP-3

The similar effects of VPS41 and AP-3 on LDCV number, morphology, behavior, and composition suggest that the two proteins may operate through a common biochemical pathway in mammals as well as yeast (Nickerson et al., 2009). To test this possibility, we knocked down both AP-3 and VPS41. RNAi targeting both proteins did not produce any effect on the regulated secretion of transfected ANF-GFP (Figure 3C) or of endogenous SgII (Figure S2A) greater than that observed for VPS41 alone. Importantly, VPS41 RNAi has no effect on the potency of AP-3 RNAi (Figure S2B). We also observed no additive effect of RNAi against both proteins on LDCV number (Figure 3A). Because RNAi targeting either VPS41 or AP-3 reduces LDCV number by only ~50%, the failure to observe any additional effect with knockdown of both strongly suggests that the two proteins act in the same pathway.

We then determined whether mammalian VPS41 and AP-3 interact biochemically. Because appendage domains mediate the interaction of multiple APs with other proteins including clathrin (Dell'Angelica et al., 1998; Owen et al., 2000; Knuehl et al., 2006; Schmid et al., 2006), we used GST fusions to the appendages of large AP-3 subunits β and δ in a "pull-down" experiment with epitope-tagged rat VPS41 expressed in COS cells (Figure 3D). We find that the δ appendage (residues 720–1,204) pulls down VPS41, but the appendages of ubiquitous subunit β3A and neural-specific β3B pull down much less, indicating specificity for the δ subunit. We also observed that the δ hinge (residues 650–797) is sufficient to mediate this interaction (Figure 3D), and this is the same domain required for the binding of AP-3 δ to VAMP7 (Kent et al., 2012). Moreover, we find that GST fusions to the appendage of δ pull down a mutant containing residues 1–595 that lacks the C terminus of VPS41 (ΔC) but not an N-terminal deletion mutant (residues 162–853) (ΔN) (Figure 3E). The analysis of further deletions indicates that binding occurs within residues 1 to 36 (Figure 3F). The hinge region of the δ appendage thus binds specifically to the extreme N terminus of VPS41, which contains a PEST sequence very similar to that found required for interaction with AP-3 in yeast VPS41 (Cabrera et al., 2010).

VPS41 RNAi Impairs Regulated Exocytosis of NPY-pHluorin by Hippocampal Neurons

To determine whether VPS41 influences LDCV formation in primary culture, we knocked down its expression in rat hippocampal neurons using shRNA sequences previously

validated in PC12 cells (Figure 4A). Using an LDCV cargo protein (neuropeptide Y) fused to the ecliptic pHluorin, a form of GFP quenched at the acidic pH of organelles such as LDCVs (Zhu et al., 2007), we monitored LDCV exocytosis from dissociated cultures of live, transfected neurons. Stimulating release by field stimulation at 30 Hz for 45 s, we observed many individual exocytotic events in the axons of control neurons transfected with control shRNA (Figure 4B) and many fewer events in cells transfected with VPS41 shRNA (Figure 4C). The total number of NPY-pHluorin puncta did not change between the two conditions (Figure 4D), and normalization to the total number of puncta in each condition showed a dramatic reduction in stimulated events with VPS41 RNAi relative to control (Figure 4E). Normalization to axon length confirmed the reduction in exocytotic events with VPS41 knockdown (Figure 4F).

VPS41 Self-Assembles into a Lattice

VPS41 contains a single clathrin heavy chain repeat (CHCR) in its C-terminal domain (Ybe et al., 1999). Clathrin comprises eight of these repeats and they are located at leg regions that mediate self-assembly, raising the possibility that like clathrin, VPS41 could self-assemble to function as a coat protein. To determine whether VPS41 can form a lattice, we expressed full-length recombinant mammalian VPS41 in Sf9 insect cells using baculovirus, purified the protein by metal affinity chromatography and removed any remaining contaminants by size exclusion chromatography (Figure 5A).

To monitor self-assembly, we first used a light-scattering assay that has previously been used to study clathrin. Very similar to the central hub domain of clathrin (Liu et al., 1995), we find that a drop in pH from 7.9 to 6.5 leads to a rapid, persistent increase in light scattering by recombinant human VPS41 (Figure 5B). Increasing pH back to ~7.9 reverses the increase in light scattering, effectively excluding denaturation and aggregation. The highest pH that will promote VPS41 assembly appears to be ~7.2 (Figure 5C), also very similar to the self-assembly properties of the clathrin hub fragment in the absence of regulatory light chain subunits (Liu et al., 1995). We further observed that increasing salt concentration inhibits self-assembly (Figure 5B), suggesting that charged interactions play a role in the process.

To determine whether self-assembly of VPS41 depends on its CHCR, we expressed and purified a mutant that lacks the C-terminal domain where the CHCR is located (Figure S3A). The mutant does not show any pH-dependent change in light-scattering, even when the pH is lowered to 6.5 (Figure 5D). The self-assembly of VPS41 monitored by light scattering thus depends on the CHCR domain.

We then used negative stain EM to characterize the structures formed by human VPS41 in vitro. As anticipated for the protein at high pH, images of negative-stained VPS41 showed mostly monodispersed particles (Figure 5E). At low pH, however, we observed relatively large particles with apparent lattices. The size of the particles was not uniform, but the meshwork appearance suggests a coat-like assembly that could potentially drive membrane invagination. Notably, similar irregular meshwork structures are generated by self-assembly of clathrin hub fragments, which also form structures of variable dimensions that lack the directed assembly of full-length clathrin (Liu et al., 1995). Our morphological analysis thus shows that purified, recombinant VPS41 can form an irregular lattice in vitro with clathrin-like properties, supporting its role as a coat protein in vivo.

To determine how VPS41 might assemble, we examined the unassembled structures that occur at high pH. Representative two-dimensional class averages calculated from negatively stained VPS41 particles at high pH showed two major types of particle (Figures 5F and S3C). Type I particles have a C-shape and may represent monomeric VPS41 interacting

head-to-tail. In contrast, the dimension of elongated type II particles suggests that they correspond to an oligomer of VPS41, very likely a dimer. Indeed, this estimate is consistent with the size-exclusion profile of full-length VPS41, which migrates at ~250 kDa (Figure 5A). In addition, most of the type II particle class averages exhibit globular heads at each end that are connected by floppy tails. Because the N terminus of VPS41 is predicted to fold as a β-propeller and the C terminus as an alpha-solenoid (Plemel et al., 2011), we speculate that the globular heads correspond to the N-termini of individual VPS41 molecules that interact at their C-terminal tails, presumably through the CHCR motif. Consistent with this, the VPS41 deletion mutant lacking the CHCR migrates as a monomer by size-exclusion chromatography (Figure S3A) and appears globular by EM (Figure S3B). In contrast to the clathrin triskelion, the basic element of the VPS41 coat thus appears to be a dimer.

We assessed the interaction of VPS41 with itself by coimmunoprecipitation. Using VPS41 constructs tagged with either HA or myc epitopes and cotransfected into COS cells, we find that antibodies to myc can precipitate the HA-tagged protein but only when the myc-tagged protein is present (Figure 5G). VPS41 can thus recognize itself in vivo and in vitro, presumably through the CHCR-containing domain.

To determine whether regulated secretion depends on the assembly of VPS41 and its interaction with AP-3, we tested the functionality of a C-terminal truncation mutant lacking the CHCR domain required for self-assembly and an N-terminal truncation (ΔN36) mutant lacking the AP-3 binding site (Figure 6A). Figure 6B shows that deletion of the CHCR domain (ΔC) eliminates the rescue of regulated secretion by VPS41. Western analysis further shows that wild-type and ΔC VPS41 are expressed at equivalent levels (Figure 6C). The role of VPS41 in formation of the regulated pathway thus depends on the CHCR and by inference, its capacity for self-assembly. We also observed that the ΔN36 mutant defective in AP-3 binding increases but does not fully rescue regulated secretion (Figure 6D), possibly because this mutant, although defective, can still assemble with residual endogenous VPS41.

To assess a role for VPS41 in coat formation by cells, we used a genetically encoded tag for ultrastructural localization. On exposure to light and oxygen, a polypeptide derived from the blue light-sensing plant protein phototropin generates singlet oxygen, and singlet oxygen reacts with diaminobenzidine (DAB) to produce an electron-dense deposit (Shu et al., 2011). DAB limits the diffusion of singlet oxygen, resulting in a highly localized deposit, which can then be imaged at high resolution by standard EM. Thus, we fused this mini singlet oxygen-generating protein (miniSOG) to the N terminus of RNAi-resistant VPS41 and expressed it in PC12 cells after knockdown of the endogenous protein. It is important to note that the miniSOG tag does not change the overall distribution of VPS41 by immunofluorescence. In particular, miniSOG-VPS41 showed a punctate distribution in transfected PC12 cells that colocalizes with the lysosomal protein lamp-1, very similar to VPS41 tagged with an HA epitope alone (Figures S4A and S4B). For the ultra-structural analysis, we exposed the fixed cells to blue light and oxygen in the presence of DAB and examined thin sections by EM. In ~100 cells transfected with control (cytosolic) miniSOG, we did not find any deposits associated with membranes (Figure 7B). In contrast, ~25% of the cells expressing miniSOG-VPS41 showed deposits. They form around vesicles budding from the Golgi complex, generally at the end of stacks (Figure 7A, arrowheads). A miniSOG construct fused to the C terminus of VPS41 labels very similar structures (data not shown), supporting a role for VPS41 in vesicle formation at this site. In addition, we observed larger, clustered vesicles often surrounded by a regular array of electron-dense puncta (Figure S4C). Although many of the clustered vesicles exhibited a single limiting membrane, others contained double membranes (Figure S4C) similar to the LAMP1 carriers recently described (Pols et al., 2013). However, these vesicles differ considerably in size and shape from those observed on the Golgi stacks and resemble structures observed with other miniSOG fusions

(J. Heuser, personal communication). These structures may thus reflect an indirect response to the miniSOG fusion, perhaps due to oxidative stress produced by singlet oxygen generation. Nonetheless, their presence correlated with expression of the miniSOG-VPS41 fusion protein and they were not observed after expression of miniSOG alone, suggesting that they are variably induced by different constructs, but may still not represent specific labeling.

DISCUSSION

The results show that among AP-3-associated proteins, VPS41 is specifically required for sorting to the regulated secretory pathway. In the absence of VPS41, release is dysregulated and LDCVs still form but in reduced numbers, with abnormal morphology and altered membrane protein composition. VPS41 thus contributes to the formation of LDCVs. The effects of VPS41 RNAi on the regulated secretory pathway also show remarkable similarity to those produced by the loss of AP-3, and the effects of VPS41 and AP-3 RNAi are not additive. The two proteins thus function in the same process.

Because LDCVs form at the Golgi apparatus, the role for AP-3 in LDCV formation differs from that previously ascribed to mammalian AP-3 within the endolysosomal pathway (Raposo and Marks, 2007; Dell'Angelica, 2009). Remarkably, we now find that another AP-3-interacting protein has exactly the same effect on LDCV formation and hence within the biosynthetic pathway. However, yeast AP-3 contributes to an alternative pathway from the biosynthetic pathway to the vacuole used by membrane proteins such as alkaline phosphatase (ALP) (Cowles et al., 1997; Odorizzi et al., 1998) that resembles LDCV formation in several respects. The sorting of multiple cargoes to this alternative vacuole pathway in yeast and *Drosophila* depends on a dileucine motif with upstream acidic residues, similar to those in VMAT and phogrin (Darsow et al., 1998; Li et al., 2005; Torii et al., 2005; Swetha et al., 2011). In addition, the ALP vacuole targeting pathway requires VPS41 as well as AP-3, and the two proteins interact biochemically as well as functionally (Rehling et al., 1999; Darsow et al., 2001). Despite the reported differences between the roles of AP-3 in model organisms and mammals, the roles of AP-3 and VPS41 in yeast and LDCV formation thus appear remarkably conserved.

The role of VPS41 in formation of the regulated pathway nonetheless differs in important respects from that previously described in yeast. First, the formation of functional LDCVs does not require fusion with the endocytic pathway. LDCVs can fuse with each other, but this is not required for regulated exocytosis (Tooze and Huttner, 1990). Second, and presumably because LDCVs do not require fusion to the endocytic pathway, the role of AP-3 and VPS41 in LDCV formation does not require other members of the HOPS complex, which mediate fusion to the vacuole in yeast. Consistent with the previous work in model organisms (Sevrioukov et al., 1999; Pulipparacharuvil et al., 2005; Akbar et al., 2009; Nickerson et al., 2009; Swetha et al., 2011), loss of either VPS39 or 41 impairs lysosomal function in mammalian cells. However, only loss of VPS41 dysregulates secretion, demonstrating the effectiveness of the knockdown and arguing against an indirect effect of endolysosomal disturbance on the regulated pathway.

Independence from the other HOPS complex subunits further suggests that the role for VPS41 in LDCV formation differs in mechanism from its role in delivery to the endocytic pathway. Recent work in yeast has focused on the role of the HOPS complex in tethering and fusion of Golgi-derived transport vesicles with the vacuole (Angers and Merz, 2009; Cabrera et al., 2009, 2010; Plemel et al., 2011). However, previous work had also implicated VPS41 earlier in the pathway from Golgi to vacuole, suggesting a role in the formation of transport vesicles (Rehling et al., 1999). We now find that recombinant, purified mammalian

VPS41 assembles reversibly at low pH, this process depends on the CHCR domain, and VPS41 lacking the CHCR domain cannot rescue the effects of VPS41 RNAi. Previous work had reported a high molecular weight form of yeast VPS41, but the nature of this species was unclear (Darsow et al., 2001). The reversible self-assembly and lattice formation now suggest that VPS41 has the potential to function as a coat protein.

Previous work has not detected a coat on budding LDCVs, but it remains possible that a coat has eluded detection by standard EM. Consistent with a role for VPS41 in this process, recent immuno-EM has localized VPS41 to the TGN and TGN-derived LAMP-1$^+$ carrier vesicles destined for the lysosome (Pols et al., 2013). To determine whether VPS41 itself forms a coat, we have used a miniSOG fusion capable of localizing VPS41 at high resolution (Shu et al., 2011). The label deposits on membrane buds at the periphery of Golgi stacks, where LDCVs are known to form, consistent with a role as coat protein. However, it is important to note that vesicles with a dense core still form in the absence of AP-3 (Asensio et al., 2010) and VPS41, suggesting that these proteins may contribute specifically to sorting rather than vesicle formation.

We also observe deposits forming a regular, periodic structure that surrounds fully formed vesicles. Several of these vesicles contain double membranes, characteristic of LAMP-1$^+$ carrier vesicles previously shown to contain VPS41. In addition, overexpression of VPS41 has been shown to induce vesicle clustering very similar to what we have observed here with overexpression of the miniSOG-VPS41 fusion (Pols et al., 2013). These structures differ considerably from those observed on the Golgi stacks and may reflect a distinct role for VPS41 as part of the HOPS complex. However, the observation that similar structures form with other miniSOG fusions suggests that they may well represent an indirect response to the expression of miniSOG, presumably due to oxidative stress.

In contrast to clathrin, VPS41 contains a single CHCR, raising questions about how it assembles into a lattice. To identify the basic unit, we have thus imaged single, unassembled particles at high pH. The analysis reveals at least two distinct types, with the smaller, C-shaped, presumably monomeric type I particle perhaps interacting with itself. Indeed, this “closed” conformation may serve to regulate assembly of VPS41 in the same way that clathrin light chain regulates assembly of the heavy chain (Liu et al., 1995), and we have indeed observed a biochemical interaction between N and C termini (data not shown). Type II particles apparently represent dimers, with the globular heads corresponding to the predicted N-terminal β-propeller of VPS41 and the two C termini linked by CHCRs. This dimer orientation differs from the clathrin triskelion and suggests that the VPS41 lattice may adopt a very different structure.

In conclusion, VPS41 acts as a coat protein for AP-3 in formation of the regulated secretory pathway. VPS41 also contributes to lysosomal trafficking, but acts independently in LDCV formation, defining an unanticipated role for the protein, and by inference AP-3, in a cellular process central to metazoan physiology, behavior, and development. Consistent with these roles, recent work has shown that *vps41* knockout mice die early in utero, apparently due to deregulated signaling by growth factors although the relative contribution of endolysosomal trafficking and regulated pathway defects to the phenotype remains unclear (Aoyama et al., 2012). We now find that loss of VPS41 also impairs the regulated release of neural peptides from neurons, with important implications for behavior and neuropsychiatric disease as well as development.

EXPERIMENTAL PROCEDURES

Cell Culture

Drosophila S2 cells were transfected with Fugene HD and PC12 and COS7 cells with Lipofectamine 2000.

Secondary Screen and Analysis

S2 cells transfected with GFP-dVMAT-HA were treated in 96-well plates with dsRNA prepared as previously described (Asensio et al., 2010). After growth for 72 hr, the cells were again treated with the same dsRNA, incubated an additional 72 hr, and surface HA expression determined by adding external HA.11 antibody bound to Zenon Alexa 647 (1:1,000) for 2 hr in standard medium, removing the unbound antibody with two washes, and subjecting the cells to high-throughput flow cytometry (lsrII, BD Biosciences) for both GFP and Alexa 647 fluorescence. The ratio of Alexa 647 to GFP fluorescence was calculated for individual cells and the mean ratio calculated from all cells in the well.

In each experiment, the cumulative frequency distribution of fluorescence ratios from individual cells was plotted, compared to control RNAi, and statistical significance analyzed by Kolmogorov-Smirnov. We applied the stringent Bonferroni correction for 18 samples (16 samples + AP-3 + negative control) and considered as positive a p value < 0.003 in at least two independent experiments.

Secretion Assays

S2 cells transfected with ANF-GFP were washed with PBS, resuspended in Tyrode's medium (in mM: 119 NaCl, 2.5 KCl, 2 CaCl2, 2 $MgCl_2$, 30 glucose, 25 HEPES [pH 7.4]), split equally into two tubes, incubated in the presence or absence of 100 μg/ml LPS (Sigma-Aldrich) for 1 hr at 27°C, sedimented, and the fluorescence from 200 μl aliquots of the supernatant measured in triplicate using a plate reader (Tecan), with stimulated secretion expressed as a percent of the respective unstimulated condition.

siRNAs were transfected twice (at 50 nM) 3 days apart, the PC12 cells washed 2–3 days later and incubated in Tyrode's buffer containing 2.5 mM K^+ (basal) or 90 mM K^+ (stimulated) for 30 min at 37°C. The supernatant was then collected, cell lysates prepared as previously described (Asensio et al., 2010), and the samples analyzed by quantitative fluorescent immunoblotting.

Density Gradient Fractionation

Equilibrium sedimentation through sucrose was performed as previously described (Waites et al., 2001). Briefly, a postnuclear supernatant was prepared from PC12 cells by homogenization at 8 μm clearance with a ball bearing device, loaded onto a 0.6 M–1.6 M continuous sucrose gradient, and sedimented at 30,000 rpm in an SW41 rotor for 14–16 hr at 4°C. Fractions (~200 μl each) were collected from the top directly into a 96-well plate (Costar) and ANF-GFP fluorescence read using a plate reader (Tecan). For SgII, p38, and Syt1, pools of four fractions were analyzed by quantitative fluorescent immunoblotting.

Electron Microscopy

PC12 cells grown on aclar discs were fixed in 2.5% glutaraldehyde and processed as previously described (Asensio et al., 2010). The photo-oxidation reaction was also performed as described before (Shu et al., 2011), using a blue LED at 200 mW/cm^2 for 60–90 min.

Neuronal Culture and Live Imaging

Dissociated cultures of postnatal rat hippocampal neurons were transfected with NPY-pHluorin, mCherry-synaptophysin and the pJHUB vector encoding either control or VPS41 shRNA along with the blue fluorescent protein (Tracy et al., 2011) and imaged as previously described (Onoa et al., 2010), stimulating at 30 Hz for 45 s in the presence of CNQX and APV. All procedures involving animals were approved by the University of California-San Francisco Institutional Animal Care and Use Committee.

Pull-Down Assays

The appendage domains of rat AP-3 delta, beta3A, and beta3B were amplified by PCR and cloned in-frame into pGEX-4T1. The recombinant proteins were induced for 14 hr at 22°C in *Escherichia coli* BL21 (DE3) using 0.1 mM IPTG. The bacteria were lysed by sonication and GST fusions purified by incubation with glutathione-Sepharose beads (GE Healthcare Life Sciences) and elution with 10 mM glutathione in 50 mM Tris, pH 8.0. COS7 cells were lysed in 50 mM Tris, pH 7.4, 50 mM NaCl, 1 mM EDTA, 1 mM DTT, 1% TX-100, 1 mM PMSF, and complete protease inhibitors (Roche) for 30min at 4°C with gentle shaking, followed by centrifugation at 16,000 × *g* for 10 min. Pull-down assays were performed by incubating 100 μg GST fusions prebound to glutathione-Sepharose beads for 1 hr at 4°C with COS7 lysates.

Protein Purification

Three days after infection with baculoviruses produced according to the manufacturer's instructions (Invitrogen), Sf9 cells were harvested by centrifugation and resuspended in binding buffer (50 mM Tris, 500 mM NaCl, 7.5 mM imidazole, pH 8.0) with 1 mM PMSF and protease inhibitors (Complete, Roche). The cells were lysed by sonication and the debris pelleted for 1 hr at 42,000 rpm in a 70Ti rotor. Supernatants were passed through a 0.2 μm filter and incubated with Ni-Nta agarose (QIAGEN) for 1 hr at 4°C. The agarose was then washed five times in binding buffer with 40 mM imidazole and His-hVPS41 eluted with 250 mM imidazole. The eluates were immediately loaded onto a Superdex size exclusion column. Fractions containing pure His-hVPS41 were concentrated by centrifugation through an Amicon filter (50 kDa cutoff).

Assembly Assays

To remove any aggregates, all purified proteins were sedimented at 75,000 rpm in a TLA 100.2 rotor at 4°C for 10 min before use. One hundred microliters of purified protein at ~100 ng/μl in 10 mM Tris, pH 8.0 was used to monitor self-assembly by light scattering (at 320 nm). Assembly was induced by adding 4 μl 1 M MES buffer at the indicated pH and disassembly by adding 4 μl 1 M Tris pH 9.0, as previously described (Liu et al., 1995).

Negative-Staining Single Particle EM

Purified sample (2.5 μl) was absorbed onto glow-discharged, carbon-coated copper grids, washed in appropriate pH buffer, then stained in 0.75% aqueous uranyl formate. Grids were imaged at room temperature using a FEI Tecnai T12 electron microscope with an LaB6 filament and operated at an acceleration voltage of 120 kV. Unless otherwise specified, images were taken at a magnification of 52,000×with a defocus −1.5 μm on a 4,000 × 4,000 UltraScan CCD (Gatan) using low-dose procedures.

A total of ~1,600 particles were selected manually, then subjected to one cycle of reference-free alignment and classification. Unique classes averages were selected and used as references for a further five cycles of multireference alignment.

Statistics

Unless indicated otherwise, all statistical analysis was performed using the two-tailed Student's t test.

Supplementary Material

Refer to Web version on PubMed Central for supplementary material.

Acknowledgments

We thank Reena Zalpuri and the UC Berkeley EM Laboratory for their help with the EM and the members of the Edwards laboratory for thoughtful discussion, the Swiss National Science Foundation and Feldman Family Foundation for support to C.S.A., the Bumpus Foundation for a fellowship to J.M., the UCSF Program for Breakthrough Biomedical Research (New Technology Award to Y.C.), and the National Institutes of Health for support to D.W.S. (MH085406), F.M.B. (GM038093), and R.H.E. (DA10154 and MH096863).

References

Akbar MA, Ray S, Krämer H. The SM protein Car/Vps33A regulates SNARE-mediated trafficking to lysosomes and lysosome-related organelles. Mol Biol Cell. 2009; 20:1705–1714. [PubMed: 19158398]

Angers CG, Merz AJ. HOPS interacts with Apl5 at the vacuole membrane and is required for consumption of AP-3 transport vesicles. Mol Biol Cell. 2009; 20:4563–4574. [PubMed: 19741093]

Aoyama M, Sun-Wada GH, Yamamoto A, Yamamoto M, Hamada H, Wada Y. Spatial restriction of bone morphogenetic protein signaling in mouse gastrula through the mVam2-dependent endocytic pathway. Dev Cell. 2012; 22:1163–1175. [PubMed: 22698281]

Arvan P, Castle D. Sorting and storage during secretory granule biogenesis: looking backward and looking forward. Biochem J. 1998; 332:593–610. [PubMed: 9620860]

Asensio CS, Sirkis DW, Edwards RH. RNAi screen identifies a role for adaptor protein AP-3 in sorting to the regulated secretory pathway. J Cell Biol. 2010; 191:1173–1187. [PubMed: 21149569]

Bauerfeind R, Jelinek R, Hellwig A, Huttner WB. Neurosecretory vesicles can be hybrids of synaptic vesicles and secretory granules. Proc Natl Acad Sci USA. 1995; 92:7342–7346. [PubMed: 7638193]

Blagoveshchenskaya AD, Hewitt EW, Cutler DF. A complex web of signal-dependent trafficking underlies the triorganellar distribution of P-selectin in neuroendocrine PC12 cells. J Cell Biol. 1999; 145:1419–1433. [PubMed: 10385522]

Blagoveshchenskaya AD, Hannah MJ, Allen S, Cutler DF. Selective and signal-dependent recruitment of membrane proteins to secretory granules formed by heterologously expressed von Willebrand factor. Mol Biol Cell. 2002; 13:1582–1593. [PubMed: 12006654]

Cabrera M, Ostrowicz CW, Mari M, LaGrassa TJ, Reggiori F, Ungermann C. Vps41 phosphorylation and the Rab Ypt7 control the targeting of the HOPS complex to endosome-vacuole fusion sites. Mol Biol Cell. 2009; 20:1937–1948. [PubMed: 19193765]

Cabrera M, Langemeyer L, Mari M, Rethmeier R, Orban I, Perz A, Bröcker C, Griffith J, Klose D, Steinhoff HJ, et al. Phosphorylation of a membrane curvature-sensing motif switches function of the HOPS subunit Vps41 in membrane tethering. J Cell Biol. 2010; 191:845–859. [PubMed: 21079247]

Cowles CR, Odorizzi G, Payne GS, Emr SD. The AP-3 adaptor complex is essential for cargo-selective transport to the yeast vacuole. Cell. 1997; 91:109–118. [PubMed: 9335339]

Darsow T, Burd CG, Emr SD. Acidic di-leucine motif essential for AP-3-dependent sorting and restriction of the functional specificity of the Vam3p vacuolar t-SNARE. J Cell Biol. 1998; 142:913–922. [PubMed: 9722605]

Darsow T, Katzmann DJ, Cowles CR, Emr SD. Vps41p function in the alkaline phosphatase pathway requires homo-oligomerization and interaction with AP-3 through two distinct domains. Mol Biol Cell. 2001; 12:37–51. [PubMed: 11160821]

Dell'Angelica EC, Klumperman J, Stoorvogel W, Bonifacino JS. Association of the AP-3 adaptor complex with clathrin. Science. 1998; 280:431–434. [PubMed: 9545220]

Dell'Angelica EC. AP-3-dependent trafficking and disease: the first decade. Curr Opin Cell Biol. 2009; 21:552–559. [PubMed: 19497727]

Eaton BA, Haugwitz M, Lau D, Moore HP. Biogenesis of regulated exocytotic carriers in neuroendocrine cells. J Neurosci. 2000; 20:7334–7344. [PubMed: 11007891]

El Meskini R, Galano GJ, Marx R, Mains RE, Eipper BA. Targeting of membrane proteins to the regulated secretory pathway in anterior pituitary endocrine cells. J Biol Chem. 2001; 276:3384–3393. [PubMed: 11060304]

Faúndez V, Horng JT, Kelly RB. A function for the AP3 coat complex in synaptic vesicle formation from endosomes. Cell. 1998; 93:423–432. [PubMed: 9590176]

Grabner CP, Price SD, Lysakowski A, Cahill AL, Fox AP. Regulation of large dense-core vesicle volume and neurotransmitter content mediated by adaptor protein 3. Proc Natl Acad Sci USA. 2006; 103:10035–10040. [PubMed: 16788073]

Kent HM, Evans PR, Schäfer IB, Gray SR, Sanderson CM, Luzio JP, Peden AA, Owen DJ. Structural basis of the intracellular sorting of the SNARE VAMP7 by the AP3 adaptor complex. Dev Cell. 2012; 22:979–988. [PubMed: 22521722]

Kim T, Tao-Cheng JH, Eiden LE, Loh YP. Chromogranin A, an "on/off" switch controlling dense-core secretory granule biogenesis. Cell. 2001; 106:499–509. [PubMed: 11525735]

Kim T, Zhang CF, Sun Z, Wu H, Loh YP. Chromogranin A deficiency in transgenic mice leads to aberrant chromaffin granule biogenesis. J Neurosci. 2005; 25:6958–6961. [PubMed: 16049171]

Knuehl C, Chen CY, Manalo V, Hwang PK, Ota N, Brodsky FM. Novel binding sites on clathrin and adaptors regulate distinct aspects of coat assembly. Traffic. 2006; 7:1688–1700. [PubMed: 17052248]

Krantz DE, Waites C, Oorschot V, Liu Y, Wilson RI, Tan PK, Klumperman J, Edwards RH. A phosphorylation site regulates sorting of the vesicular acetylcholine transporter to dense core vesicles. J Cell Biol. 2000; 149:379–395. [PubMed: 10769030]

Li H, Waites CL, Staal RG, Dobryy Y, Park J, Sulzer DL, Edwards RH. Sorting of vesicular monoamine transporter 2 to the regulated secretory pathway confers the somatodendritic exocytosis of monoamines. Neuron. 2005; 48:619–633. [PubMed: 16301178]

Liu SH, Wong ML, Craik CS, Brodsky FM. Regulation of clathrin assembly and trimerization defined using recombinant triskelion hubs. Cell. 1995; 83:257–267. [PubMed: 7585943]

Molinete M, Dupuis S, Brodsky FM, Halban PA. Role of clathrin in the regulated secretory pathway of pancreatic beta-cells. J Cell Sci. 2001; 114:3059–3066. [PubMed: 11686308]

Morvan J, Tooze SA. Discovery and progress in our understanding of the regulated secretory pathway in neuroendocrine cells. Histochem Cell Biol. 2008; 129:243–252. [PubMed: 18197413]

Newell-Litwa K, Salazar G, Smith Y, Faundez V. Roles of BLOC-1 and adaptor protein-3 complexes in cargo sorting to synaptic vesicles. Mol Biol Cell. 2009; 20:1441–1453. [PubMed: 19144828]

Nickerson DP, Brett CL, Merz AJ. VPS-C complexes: gatekeepers of endolysosomal traffic. Curr Opin Cell Biol. 2009; 21:543–551. [PubMed: 19577915]

Odorizzi G, Cowles CR, Emr SD. The AP-3 complex: a coat of many colours. Trends Cell Biol. 1998; 8:282–288. [PubMed: 9714600]

Onoa B, Li H, Gagnon-Bartsch JA, Elias LA, Edwards RH. Vesicular monoamine and glutamate transporters select distinct synaptic vesicle recycling pathways. J Neurosci. 2010; 30:7917–7927. [PubMed: 20534840]

Orci L, Ravazzola M, Amherdt M, Perrelet A, Powell SK, Quinn DL, Moore HP. The trans-most cisternae of the Golgi complex: a compartment for sorting of secretory and plasma membrane proteins. Cell. 1987; 51:1039–1051. [PubMed: 2826013]

Owen DJ, Vallis Y, Pearse BM, McMahon HT, Evans PR. The structure and function of the beta 2-adaptin appendage domain. EMBO J. 2000; 19:4216–4227. [PubMed: 10944104]

Plemel RL, Lobingier BT, Brett CL, Angers CG, Nickerson DP, Paulsel A, Sprague D, Merz AJ. Subunit organization and Rab interactions of VPS-C protein complexes that control endolysosomal membrane traffic. Mol Biol Cell. 2011; 22:1353–1363. [PubMed: 21325627]

Pols MS, van Meel E, Oorschot V, ten Brink C, Fukuda M, Swetha MG, Mayor S, Klumperman J. hVps41 and VAMP7 function in direct TGN to late endosome transport of lysosomal membrane proteins. Nat Commun. 2013; 4:1361. [PubMed: 23322049]

Pulipparacharuvil S, Akbar MA, Ray S, Sevrioukov EA, Haberman AS, Rohrer J, Krämer H. Drosophila Vps16A is required for trafficking to lysosomes and biogenesis of pigment granules. J Cell Sci. 2005; 118:3663–3673. [PubMed: 16046475]

Raposo G, Marks MS. Melanosomes—dark organelles enlighten endosomal membrane transport. Nat Rev Mol Cell Biol. 2007; 8:786–797. [PubMed: 17878918]

Rehling P, Darsow T, Katzmann DJ, Emr SD. Formation of AP-3 transport intermediates requires Vps41 function. Nat Cell Biol. 1999; 1:346–353. [PubMed: 10559961]

Robinson MS, Bonifacino JS. Adaptor-related proteins. Curr Opin Cell Biol. 2001; 13:444–453. [PubMed: 11454451]

Schmid EM, Ford MG, Burtey A, Praefcke GJ, Peak-Chew SY, Mills IG, Benmerah A, McMahon HT. Role of the AP2 beta-appendage hub in recruiting partners for clathrin-coated vesicle assembly. PLoS Biol. 2006; 4:e262. [PubMed: 16903783]

Sevrioukov EA, He JP, Moghrabi N, Sunio A, Krämer H. A role for the *deep orange* and *carnation* eye color genes in lysosomal delivery in *Drosophila*. Mol Cell. 1999; 4:479–486. [PubMed: 10549280]

Shu X, Lev-Ram V, Deerinck TJ, Qi Y, Ramko EB, Davidson MW, Jin Y, Ellisman MH, Tsien RY. A genetically encoded tag for correlated light and electron microscopy of intact cells, tissues, and organisms. PLoS Biol. 2011; 9:e1001041. [PubMed: 21483721]

Swetha MG, Sriram V, Krishnan KS, Oorschot VM, ten Brink C, Klumperman J, Mayor S. Lysosomal membrane protein composition, acidic pH and sterol content are regulated via a light-dependent pathway in metazoan cells. Traffic. 2011; 12:1037–1055. [PubMed: 21535339]

Tan PK, Waites C, Liu Y, Krantz DE, Edwards RH. A leucine-based motif mediates the endocytosis of vesicular monoamine and acetylcholine transporters. J Biol Chem. 1998; 273:17351–17360. [PubMed: 9651318]

Tooze SA, Huttner WB. Cell-free protein sorting to the regulated and constitutive secretory pathways. Cell. 1990; 60:837–847. [PubMed: 2138058]

Tooze SA, Flatmark T, Tooze J, Huttner WB. Characterization of the immature secretory granule, an intermediate in granule biogenesis. J Cell Biol. 1991; 115:1491–1503. [PubMed: 1757459]

Torii S, Saito N, Kawano A, Zhao S, Izumi T, Takeuchi T. Cytoplasmic transport signal is involved in phogrin targeting and localization to secretory granules. Traffic. 2005; 6:1213–1224. [PubMed: 16262730]

Tracy TE, Yan JJ, Chen L. Acute knockdown of AMPA receptors reveals a trans-synaptic signal for presynaptic maturation. EMBO J. 2011; 30:1577–1592. [PubMed: 21378752]

Turkewitz AP. Out with a bang! Tetrahymena as a model system to study secretory granule biogenesis. Traffic. 2004; 5:63–68. [PubMed: 14690495]

Waites CL, Mehta A, Tan PK, Thomas G, Edwards RH, Krantz DE. An acidic motif retains vesicular monoamine transporter 2 on large dense core vesicles. J Cell Biol. 2001; 152:1159–1168. [PubMed: 11257117]

Ybe JA, Brodsky FM, Hofmann K, Lin K, Liu SH, Chen L, Earnest TN, Fletterick RJ, Hwang PK. Clathrin self-assembly is mediated by a tandemly repeated superhelix. Nature. 1999; 399:371–375. [PubMed: 10360576]

Zhu D, Zhou W, Liang T, Yang F, Zhang RY, Wu ZX, Xu T. Synaptotagmin I and IX function redundantly in controlling fusion pore of large dense core vesicles. Biochem Biophys Res Commun. 2007; 361:922–927. [PubMed: 17686463]

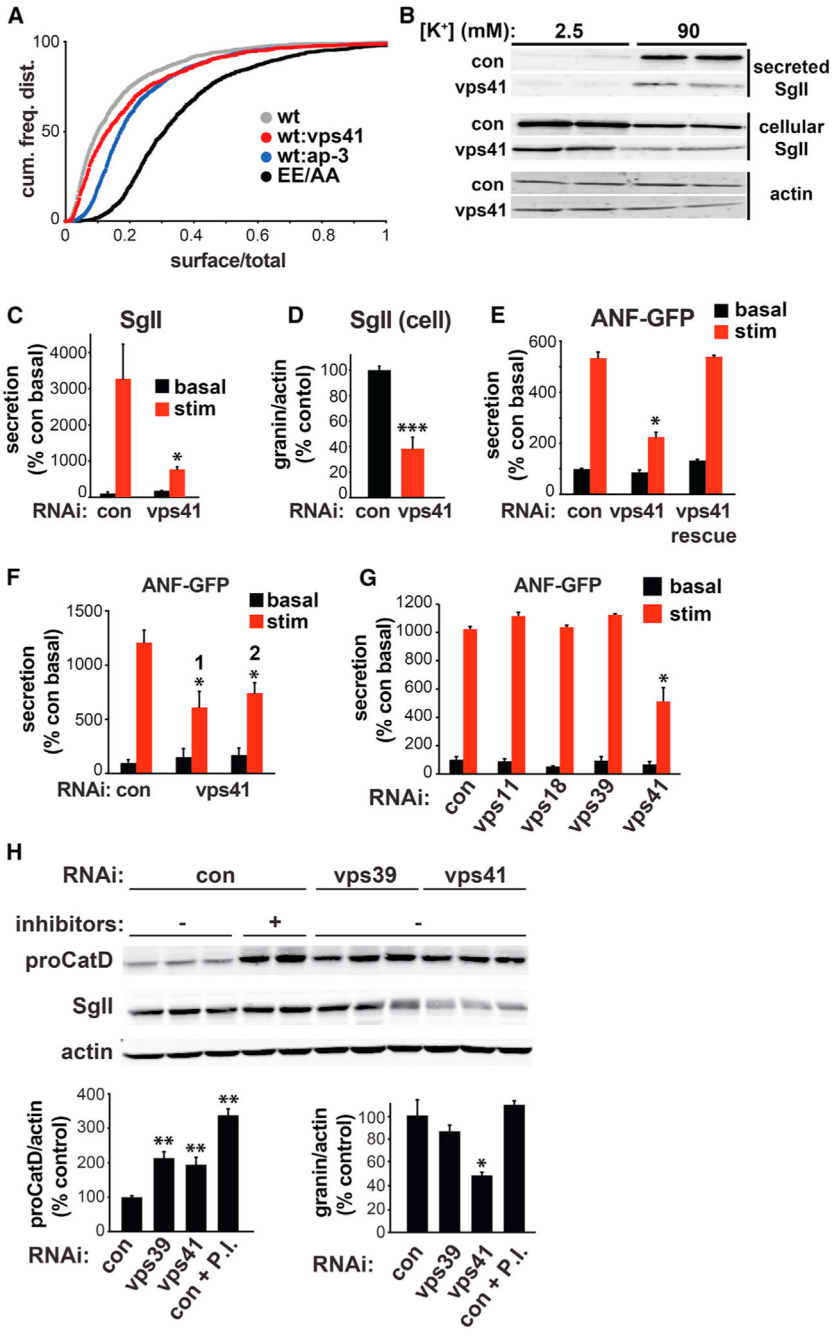

Figure 1. VPS41, but Not Other HOPS Complex Subunits, Is Required for the Regulated Secretory Pathway in PC12 Cells

(A) PC12 cells were cotransfected with EE/AA or wild-type VMAT2 (tagged with a lumenal/external HA epitope) and the siRNAs indicated, incubated for 2 hr with HA antibody conjugated to Alexa 647, washed and the fluorescence of individual cells measured by flow cytometry. The cumulative frequency distribution of surface (red)/total (green) VMAT2 shows an increase with RNAi to VPS41 as well as AP-3. $p < 10 \times 10^{-12}$ relative to wild-type control by Kolmogorov-Smirnov.

(B–D) PC12 cells were transiently transfected with either control or VPS41 siRNA, washed and incubated for 30 min in Tyrode's solution containing 2.5 mM K^+ (basal) or 90 mM K^+

(stimulated). Cellular and secreted secretogranin II (SgII) were measured by quantitative fluorescent immunoblotting (B), with the secreted SgII normalized to basal secretion in the control (C), and the cellular SgII normalized to actin (D). The immunoblots in (B) show two representative, independent samples. *$p < 0.01$ relative to stimulated secretion from control ($n = 6$); ***$p < 0.001$ relative to control ($n = 6$).

(E) PC12 cells were cotransfected with ANF-GFP as well as the indicated siRNAs in the presence (rescue) or absence of RNAi-resistant VPS41-myc, washed and incubated for 30 min in Tyrode's solution containing 2.5 mM (basal) or 90 mM (stimulated) K^+. Cellular and secreted ANF-GFP were measured using a plate reader, the results normalized to cellular content and expressed relative to basal release from the cells treated with control siRNA. *$p < 0.001$ relative to stimulated secretion from control ($n = 4–6$).

(F) PC12 cells were cotransfected with ANF-GFP and either control or VPS41 siRNAs #1 or #2 and the secretion of ANF-GFP in response to stimulation measured as described above. *$p < 0.05$ relative to stimulated secretion from control ($n = 3–4$).

(G) PC12 cells were cotransfected with ANF-GFP as well as the indicated siRNAs and stimulation-dependent ANF-GFP secretion determined as above ($n = 4$).

(H) PC12 cells were transfected with siRNA and incubated where indicated with protease inhibitors antipapain (10 μM), leupeptin (10 μM), and pepstatin A (5 μM) (P.I.) for 20 hr. Cellular proCathepsin D (proCatD) and SgII were quantified by fluorescent western analysis and the values normalized to actin immunoreactivity. *$p < 0.05$; **$p < 0.01$ relative to control ($n = 4–6$). (C–H) The data shown indicate mean ± SEM.

See also Figure S1 and Table S1.

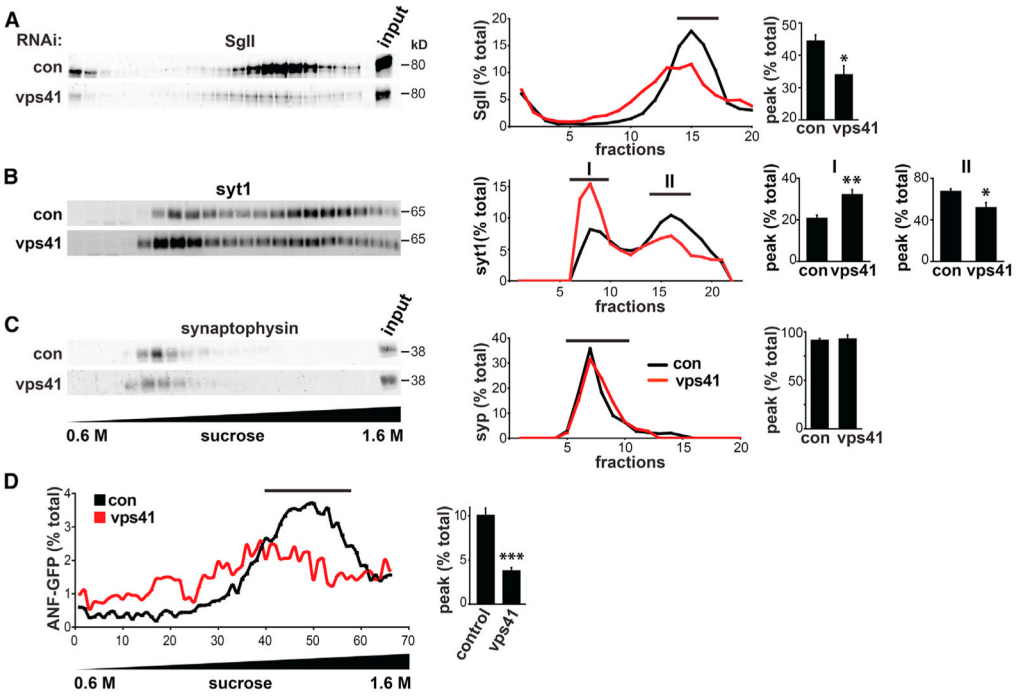

Figure 2. VPS41 RNAi Shifts LDCV Cargo to Lighter Membranes by Equilibrium Sedimentation

(A–C) PC12 cells were transfected twice with VPS41 siRNA, and the postnuclear supernatant (input) obtained 2–3 days after the second transfection was separated by equilibrium sedimentation through 0.6–1.6 M sucrose. Fractions were collected from the top of the gradient and assayed for SgII (A), synaptotagmin 1 (syt1) (B), and synaptophysin (syp) (C) by quantitative fluorescent immunoblotting. The graphs (middle) quantify multiple immunoblots of the kind shown on the left, with the immunoreactivity in each fraction expressed as a percent of total gradient immunoreactivity. Bar graphs (right) indicate the area under the relevant peak (indicated by a black line) expressed as a percent of the area under the entire curve. *$p < 0.05$; **$p < 0.01$ relative to control ($n = 3–4$).

(D) PC12 cells were cotransfected with VPS41 siRNA and ANF-GFP and the postnuclear supernatant sedimented as above. In this case, however, ~70 fractions were collected from the top of the gradient directly into a 96-well plate, and the fluorescence of ANF-GFP was measured using a plate reader. The graph indicates ANF-GFP fluorescence for each fraction expressed as percent of total gradient fluorescence. Bar graphs show the area under the curve for the peak (indicated by the black line) expressed as percent of total area. ***$p < 0.001$ relative to control by two-tailed Student's t test ($n = 3$). (A–D) The bar graphs represent mean ± SEM.

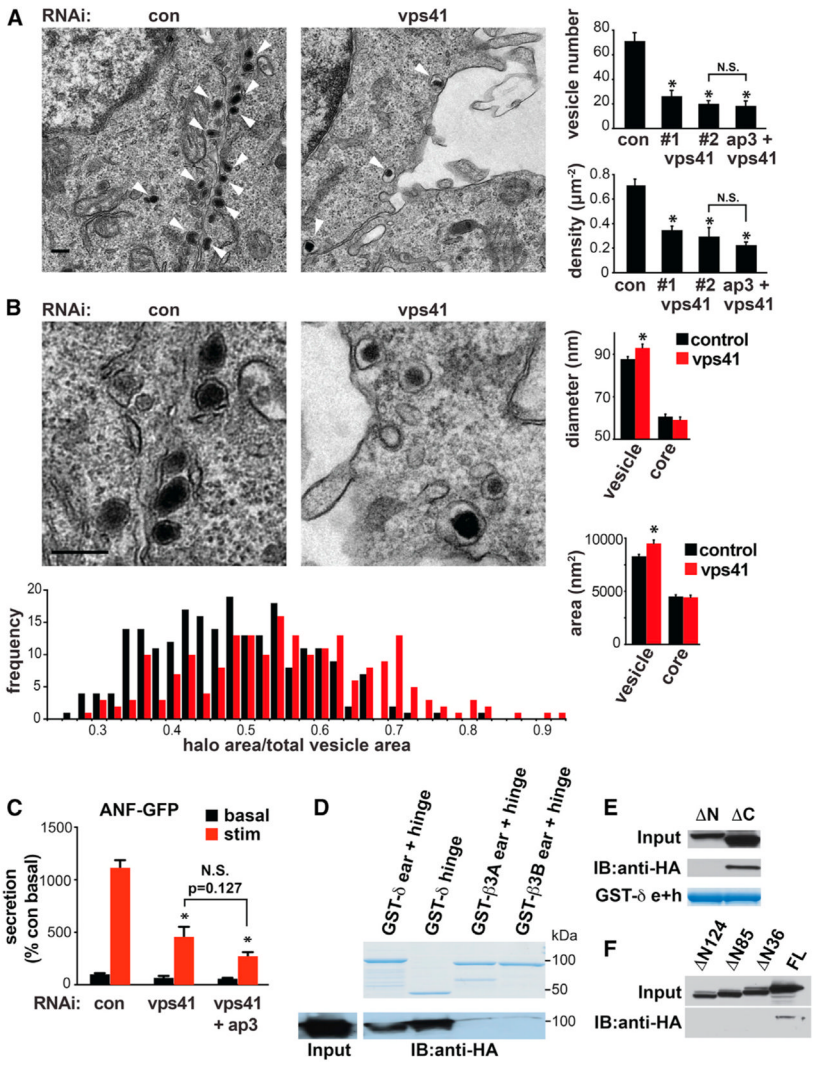

Figure 3. VPS41 Influences LDCV Morphology and Interacts with AP-3 Genetically and Biochemically

PC12 cells were transfected twice with either control, VPS41 (#1 or #2) siRNA (50 nM each), or VPS41 siRNA #2 with AP-3 siRNA (50 nM each) and processed for electron microscopy 2 days after the second transfection.

(A) Low-magnification electron micrographs show a large reduction in the number of LDCVs (arrowheads) in cells transfected with VPS41 siRNA (right) relative to controls (left). Bar graphs indicate the number of LDCVs per cell section (upper panel) and LDCV density (lower panel). *p < 0.001 relative to control (n = 20 cells/condition).

(B) Higher magnification electron micrographs show that VPS41 RNAi slightly increases the size of LDCVs, and in particular, the halo surrounding the dense core. Bar graphs indicate the diameter (upper panel) and area (lower panel) of both the entire LDCV and the electron-dense core. Subtracting the area of the core from total LDCV area yields the area occupied by the halo, and the fraction of LDCV area occupied by the halo is presented as a frequency histogram (below). *p < 0.01 from control (n = 204–221 LDCVs/condition). The scale bars represent 200 nm.

(C) PC12 cells were cotransfected with ANF-GFP as well as control, VPS41 or VPS41 with AP-3 siRNAs as indicated. ANF-GFP secretion was measured as described in Figure 1E. *p

< 0.01 relative to stimulated secretion from control (n = 4). (A–C) Bar graphs represent mean ± SEM.

(D–F) Cell lysates were prepared from COS7 cells transfected with full-length HA-VPS41 (D) or HA-VPS41 lacking the N or C terminus (E and F), incubated with GSH Sepharose-bound GST-δ ear + hinge (residues 720–1,204), GST-δ hinge (residues 650–720), GST-β3A (residues 643–1,094), or GST-β3B (residues 633–1,082) and the bound proteins eluted in sample buffer analyzed by immunoblotting for HA.

See also Figure S2.

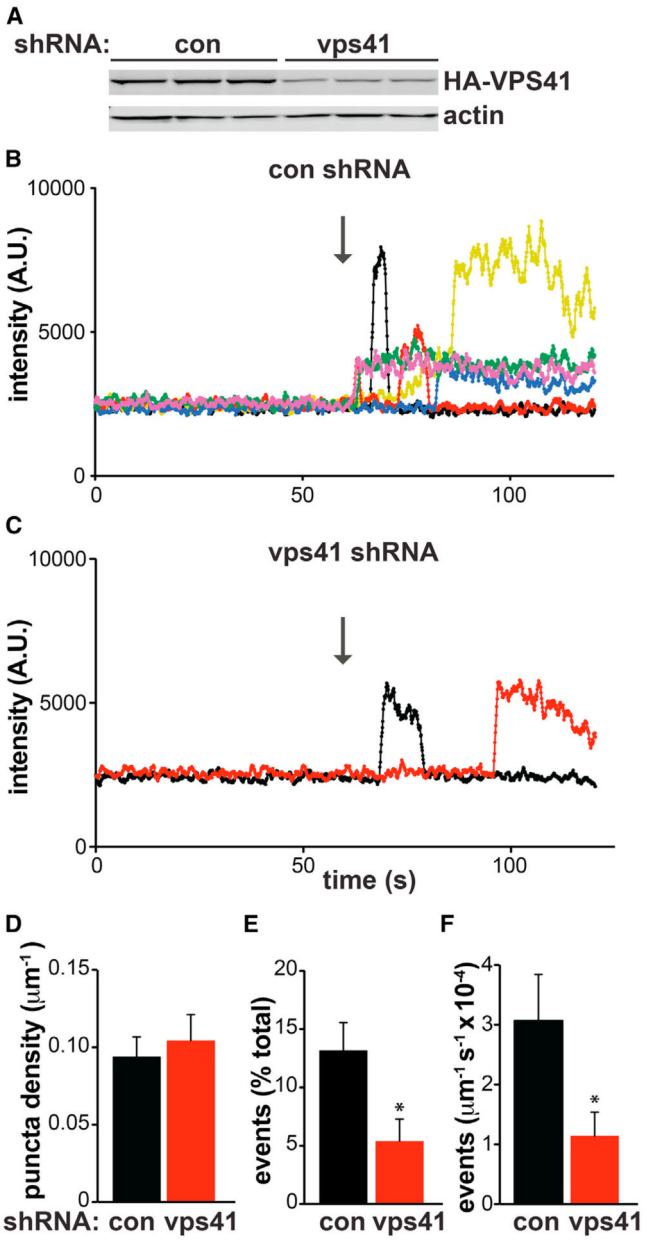

Figure 4. VPS41 RNAi Impairs Regulated Exocytosis of LDCVs by Hippocampal Neurons

(A) PC12 cells were transiently cotransfected with HA-VPS41 and either control or VPS41 shRNA. Immunoblotting the extracts for HA shows a substantial reduction with VPS41 shRNA relative to control.

(B–F) Postnatal rat hippocampal neurons were cotransfected with synaptophysin-mCherry, NPY-pHluorin, and either control or VPS41 shRNA. After 14 DIV, the cells were imaged under basal conditions for 60 s, followed by stimulation at 30 Hz for 45 s. (B and C) Representative fluorescent traces (a moving average of 10 data points) show exocytotic events in axons (identified with synaptophysin-mCherry) in response to stimulation (indicated with an arrow) for neurons transfected with control (B) or VPS41 shRNA (C). The bar graphs (D–F) quantify the live-imaging data. (D) The total number of NPY-pHluorin puncta (puncta revealed in NH_4Cl plus exocytotic events) does not change in

response to VPS41 shRNA. However, VPS41 shRNA reduces the number of stimulated NPY-pHluorin events expressed either as percent of total puncta (E) or normalized to axon length (F). *$p < 0.05$ relative to control by two-tailed Student's t test ($n = 25$). The bar graphs represent mean ± SEM.

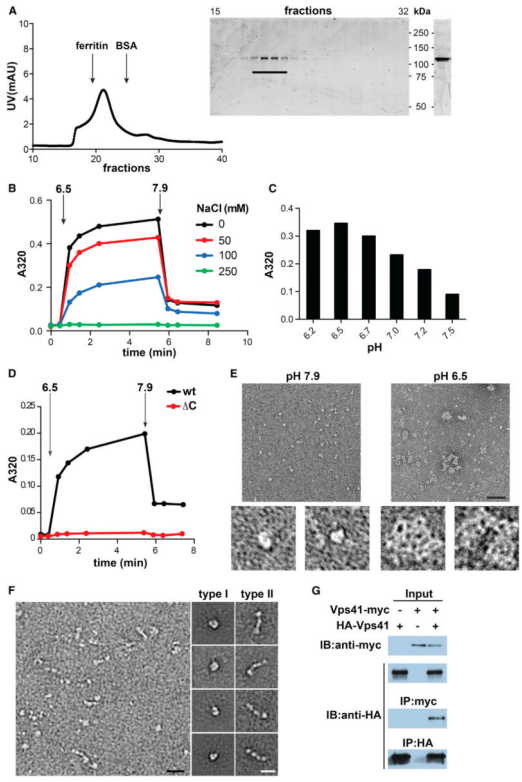

Figure 5. VPS41 Self-Assembles into a Lattice In Vitro

(A) Full-length hVPS41 was purified from Sf9 cells by metal affinity chromatography followed by gel filtration (Superdex 200) in 10 mM Tris, pH 7.9 (left). Aliquots of the collected fractions were separated by electrophoresis through polyacrylamide (SDS-PAGE) and the proteins visualized by Coomassie staining (middle). Fractions containing monomeric hVPS41 were pooled, concentrated, and again visualized by Coomassie staining after SDS-PAGE (right).

(B–D) All self-assembly reactions were performed using ~10 μg protein in a total volume of 100 μl in the absence of NaCl unless otherwise indicated. Light-scattering measurements were taken before (t = 0) and after the addition of MES, pH 6.5 (B and D) or at the indicated pH (C). After 5 min, disassembly was triggered by the addition of Tris, pH 9.0. The bar graph (C) shows the values obtained after 5 min of assembly.

(E) Negative stain EM of recombinant hVPS41 shows single particles under conditions that do not permit assembly (left, pH 7.9) and irregular lattices (right) at low pH (6.5). The panels on the bottom show single particles (left) or a lattice (right) at higher magnification. Size bar represents 50 nm.

(F) Electron micrographs of unassembled hVPS41 (left panel) reveal two main types of particle: C-shaped (type I) and elongated (type II). Representative class averages for both particle types were computed from single particles sets and are shown on the right. Size bar represents 20 nm.

(G) COS7 cells were transfected with HA-VPS41 with or without VPS41-myc, as indicated. Cell lysates were immunoprecipitated with HA antibody and samples examined by immunoblotting with anti-myc or anti-HA antibodies (lower blots). Upper immunoblots show the expression of HA-VPS41 and VPS41-myc in the cell lysates.

See also Figure S3.

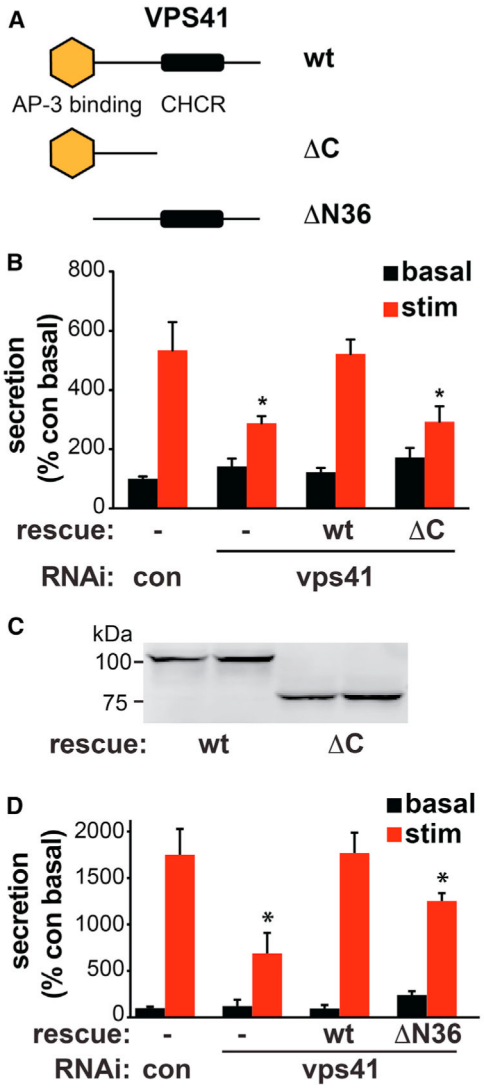

Figure 6. The VPS41 Clathrin Heavy Chain Repeat Is Required for Regulated Secretion

(A) Model of VPS41 showing the putative AP-3 binding site at the N terminus as well as the CHCR at the C terminus. The ΔC mutant contains residues 1–595 and ΔN36 residues 37–853.

(B) PC12 cells were cotransfected with control or VPS41 siRNAs, ANF-GFP, and RNAi-resistant VPS41 full-length (WT) and C-terminal deletion (ΔC) rescue constructs where indicated, and ANF-GFP secretion was measured as described in Figure 1E. *$p < 0.05$ relative to stimulated secretion from control (n = 3–4). Bar graphs represent mean ± SEM.

(C) Western analysis of the HA-tagged, RNAi-resistant constructs transfected in duplicate into PC12 cells shows equivalent expression of WT and ΔC VPS41.

(D) PC12 cells were cotransfected with control or VPS41 siRNAs, ANF-GFP, and RNAi-resistant WT or ΔN36 VPS41, and ANF-GFP secretion measured as described in Figure 1E. *$p < 0.05$ by ANOVA followed by Tukey posthoc testing, relative to stimulated secretion from control (n = 4). Bar graphs represent mean ± SEM.

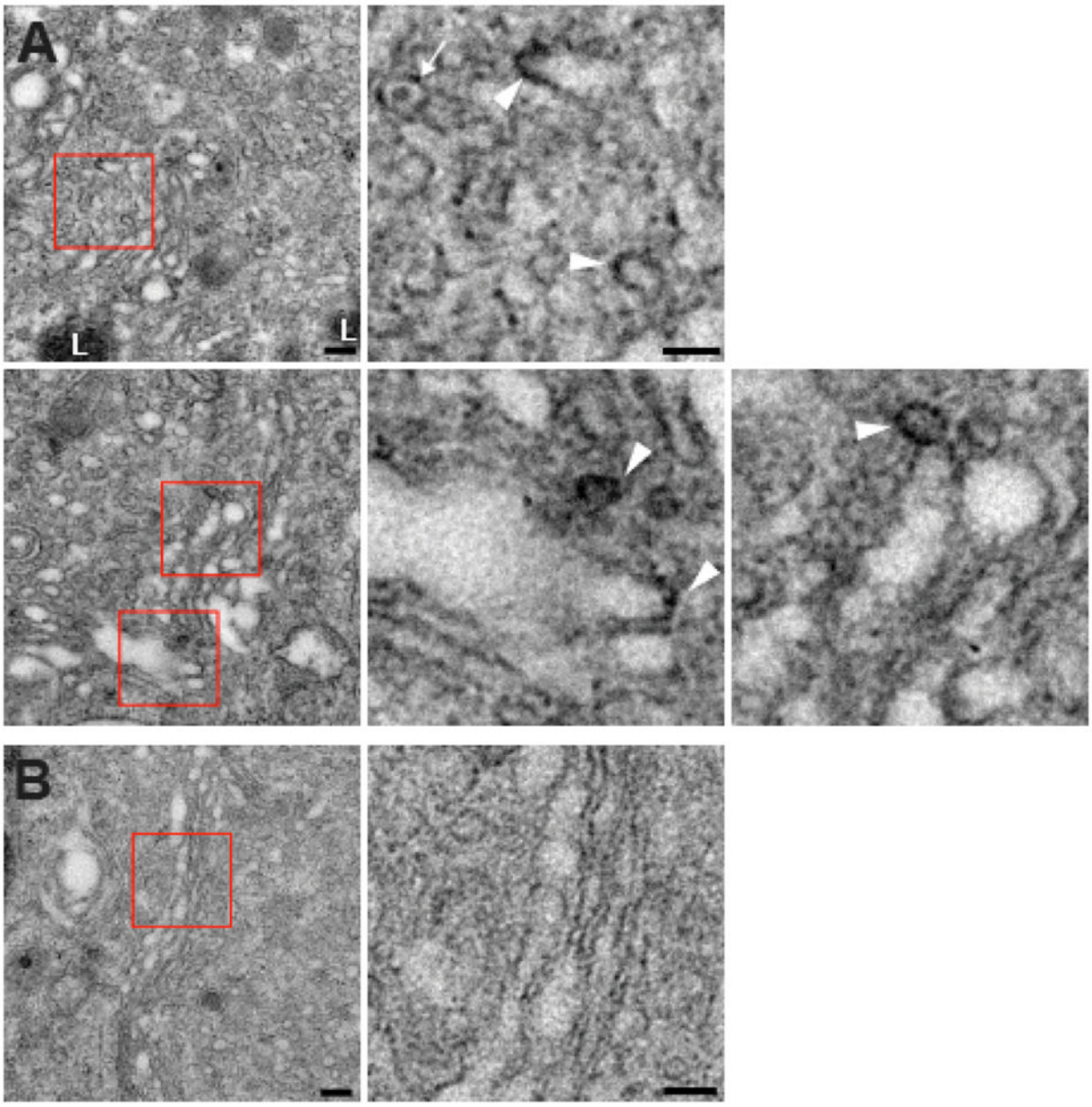

Figure 7. VPS41 Decorates Golgi-Derived Membrane Buds

PC12 cells were transfected twice with VPS41 siRNA and once with cDNA encoding either siRNA-resistant miniSOG-VPS41 (A) or cytoplasmic miniSOG (B) alone as control. Three days after the second transfection, cells were fixed, oxidized by blue light in the presence of oxygen and DAB, and processed for EM.

(A) Electron micrographs show electron-dense DAB reaction product closely apposed to membrane buds associated with the ends of Golgi cisternae in cells transfected with miniSOG-VPS41. Red boxes indicate the regions magnified to the right. The white arrowheads indicate electron-dense deposits and the white arrow an unlabeled LDCV.

(B) A cell expressing the cytoplasmic miniSOG shows an unlabeled Golgi profile. Scale bars represent 200 nm. L, lysosome.

See also Figure S4.